Raman microspectroscopy of a silicon solar cell

Jeya Prakash Ganesan, ¹ Nafis Iqbal, ¹ Fernand Torres Davila, ¹ Kristopher O. Davis, ^{1,2,3} Laurene Tetard, ^{1,4,5} and Parag Banerjee^{1,2,4,5}

¹University of Central Florida, Orlando, FL, 32816, USA.

²Florida Solar Energy Center (FSEC), University of Central Florida, Orlando, FL, 32816, USA.

³Resilient, Intelligent and Sustainable Energy Systems (RISÉS), Faculty Cluster Initiative, University of Central Florida, Orlando, FL, 32816, USA.

⁴Nanoscience Technology Center (NSTC), University of Central Florida, Orlando, FL, USA, 32816.
⁵Renewable Energy and Chemical Transformation (REACT), Faculty Cluster Initiative, University of Central Florida, Orlando, FL, 32816, USA

Abstract— A fully finished, aluminum back-surface field, multi crystalline silicon solar cell was analyzed using Raman microspectroscopy. New insights into the process and material quality of the finished device is obtained. First, the analysis helps to identify differences in the Raman spectra of the remnant saw marks on the silicon surface when compared to a textured silicon surface. Second, inclusions embedded inside the silicon surface are unambiguously identified as nanocrystalline silicon. Using confocal Raman microspectroscopy 3D tomography of the inclusions are constructed and the state of compressive stress around these particulates are measured. Third and finally, Raman analysis of the silver line shows a clear silver oxide signal that is detected up to 25 µm away from the edge of the silver line thus, quantifying the quality and effectiveness of the screen-printing and firing process. Taken together, these results demonstrate Raman microspectroscopy as a valuable tool for identification of micron-scale feature sizes and defects, otherwise too small to be identified using current metrology techniques.

Keywords—Photovoltaics, Back Surface Field, Confocal Raman

I. INTRODUCTION

Technological advances in solar cell manufacturing at economies-of-scale have led to a significant decrease in the price of solar cells. New materials and improved processes have steadily helped increase solar cell efficiencies (currently at 26.7 % for silicon (Si) solar cells) and reliability (20 years with < 5.6 % degradation in open circuit voltage ($V_{\rm oc}$)) [1]. The high-volume manufacturing environments for Si solar cells integrate processes that dope precise regions in the absorber layers, create textured surfaces that efficiently absorb solar radiation, integrate transparent conductors and metallic films onto the device, while packaging, wiring and laminating cells into modules.

Defect metrology is a vital part of the PV production process. Electroluminescence (EL) and photoluminescence (PL) are the two most common methods by which defects are identified. The significance of PL is highlighted with the following example. Fig.1A shows a cored-out, aluminum back surface field silicon solar cell. Fig. 1B shows the PL image of the same cored sample. Several cracks are observed due to the coring process. Fig. 1C shows the zoomed-in image from Fig. 1B where the red boxed region has a lower PL intensity. Beyond a lower PL intensity, there is not much by way of information that can be garnered from the PL map. However, when observed under an optical microscope the same boxed region can be identified as a region where the silicon texturing process has been incomplete, leaving behind remnant saw marks. This shows that PL, while providing rapid information

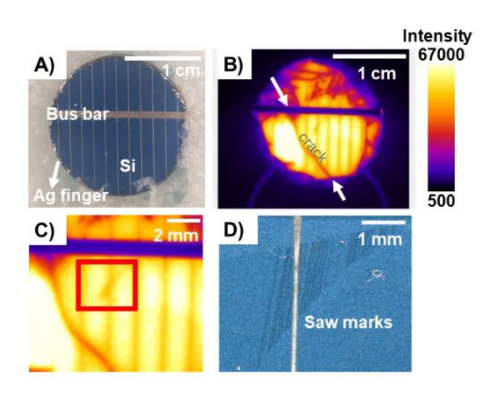


Fig. 1A. Al-BSF silicon solar cell showing busbar, Ag finger and Si layer. 1B. Photoluminescence image of the silicon solar cell. 1C. Zoomed in image of 1B with a red boxed region showing a low PL intensity area. 1D. Optical micrograph of the red boxed region showing the presence of saw marks in correlation with low PL intensity region.

of device quality, cannot identify and characterize defects at the spatial scale and resolution required for process and device quality improvements.

In this work, we demonstrate Raman microspectroscopy as a characterization tool for finished solar cells. Raman analysis, 1) provides feature information at the micron spatial scale, 2) identifies the chemical signature of materials, 3) maps mechanical stress information around defects and, 4) drives systematic process improvements (e.g., in the firing process) in the manufacturing line.

II. EXPERIMENTAL

Multi crystalline aluminum back surface field (Al-BSF) solar cell was obtained from Canadian Solar®. From top to bottom, the layers were Ag contacts, a 75 nm SiN_x layer as an anti-reflecting coating (ARC), *n*-type Si as emitter, 180 μm *p*-type Si absorber and a thick 250 μm thick Al back contact. Optical images for profilometry were taken using a Keyence® Digital Microscope VHX-5000. The instrument used to perform XY micro-Raman spectroscopy was a WITec® 300 RA microscope. The mappings were performed using a laser excitation radiation of 532 nm. The penetration depth of this laser in Si is $\sim 1.27~\mu m$. With the 20× objective used, the optical system provides a depth of focus (DOF) of 7 μm and a spot radius of 400 nm.

The spot radius of 400 nm also provides the necessary information for conducting XY mapping. For example, an area of $25 \times 25 \ \mu\text{m}^2$ was mapped with a grid size of 31×31 (i.e., a total of 961 data points) with each step 800 nm apart which is

equal to the spot diameter. Unless otherwise noted, the accumulation time was 1 second and every scan was integrated once. A larger area scan of $75\times25~\mu m^2$ with 2852 data points was performed with an objective of $20\times$ on saw marks. The laser intensity used was 20 mW. For the inclusion, an objective of $10\times$ was used on an area of $45\times45~\mu m^2$ mapped with 784 data points. The accumulation time was 2 seconds, and every scan was integrated once. The laser intensity used was 25 mW. For the Ag finger, a lower magnification using a $10\times$ objective was used, an area of $140\times140~\mu m^2$ was mapped with 2500 data points. The laser intensity used was 30 mW. Scan acquisition was conducted from 12 to 1200 cm $^{-1}$ wavenumbers using a grating with 1800 gratings/mm and a resolution of 0.3 cm $^{-1}$. Total accumulation times for obtaining area scans ranged from tens of minutes to up to 3 hours long.

To achieve true confocal imaging of the inclusion reported in this work, a Horiba® LabRam Evolution system with a 785 nm laser was used. This laser wavelength allows for a penetration depth of 10 μm . The experimental conditions for confocal mapping were 1 second integration time and 1 accumulation. A 50× long working distance (LWD) objective, 1800 gratings/mm and a laser intensity of 25 mW was used to conduct the 3D mapping. Prior to conducting any Raman measurements, the equipment were calibrated using a pristine, single crystal Si wafer with the TO phonon adjusted to 520.5 cm $^{-1}$.

III. RESULTS AND DISCUSSION

Three regions of the Al-BSF silicon solar cell is analyzed via Raman microspectroscopy. Regions with saw marks, inclusion and Ag finger are Raman analyzed and discussed.

With areal mapping of the saw marks shown in Fig. 1D, the marks do not register on both the intensity and peak position plot. This is possibly a result of the textured surface. Fig. 2 shows the distribution of the peak position and the FWHM of the Si peak. Since the areal mapping of the saw marks region is larger than the region without saw marks, the histogram for the saw marks were sampled to match the size of the region without saw marks. Both the peak position and the FWHM are shifted to a higher value for the saw marks region, indicating that in the presence of the saw marks the Si is under compressive stress. Similar Raman shifts indicating residual compressive stress have been reported when analyzing swarf from the sawing

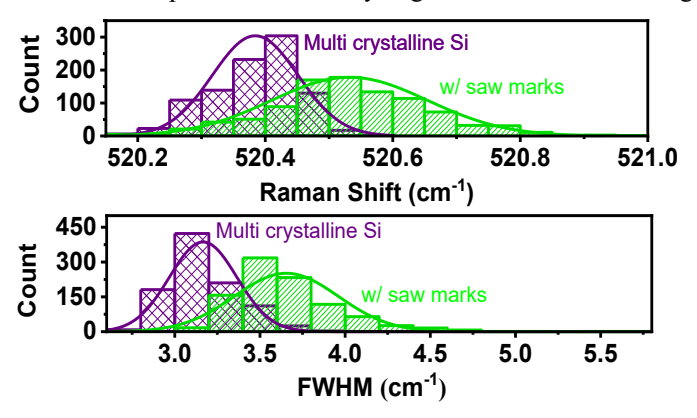


Fig. 2. The distribution of peak position and FWHM from the area mapping for the multi crystalline Si only and Si with saw marks regions.

process [2]. Further, the distributions are wider for the saw marks region. Hence, by performing statistical analysis of Raman data helps to delineate the differences between the crystalline quality.

In Fig. 3, a series of twelve individual Raman spectra are sampled across the inclusion. Each scan is 1.6 µm apart. At point just outside the inclusion, the scan consists of a sharp peak at 520.3 cm⁻¹ assigned to crystalline Si (c-Si). As the scan position moves over the inclusion, an additional broad peak appears on the lower wavenumber side. As the probe moves over the inclusion the peak position changes from 504.0 cm⁻¹ to 492.0 cm⁻¹. The broad peak subsides, and the c-Si peak sharpens again as the laser runs past the inclusion.

Peak shifts to lower wavenumbers in the TO phonon mode of the Si result from i) tensile stress, ii) phonon confinement due to nanocrystallinity or, iii) temperature changes to the sample. In the case of nanocrystalline Si (nc-Si), these effects are complex. We identify the secondary Si peak belonging to nc-Si which lies between c-Si (520.3 cm⁻¹) and the fully amorphous Si (a-Si) peak at 480.0 cm⁻¹ [3]. The inclusion represents a Si swarf – a possible remnant of the Si ingot sawing process [4]. Here, the c-Si is converted to nc-Si due to the extreme stresses involved during sawing.

The inclusion was subjected to confocal Raman mapping as it provides a non-destructive technique for observing subsurface structure and obtain a 3D map of the inclusion. The individual areal maps at different heights can be vertically stacked and represented as a 3D image as shown in Fig. 4, clearly highlighting a nanocrystalline inclusion embedded on a Si solar cell surface. The green color corresponds to the c-Si peak while the red corresponds to the nc-Si.

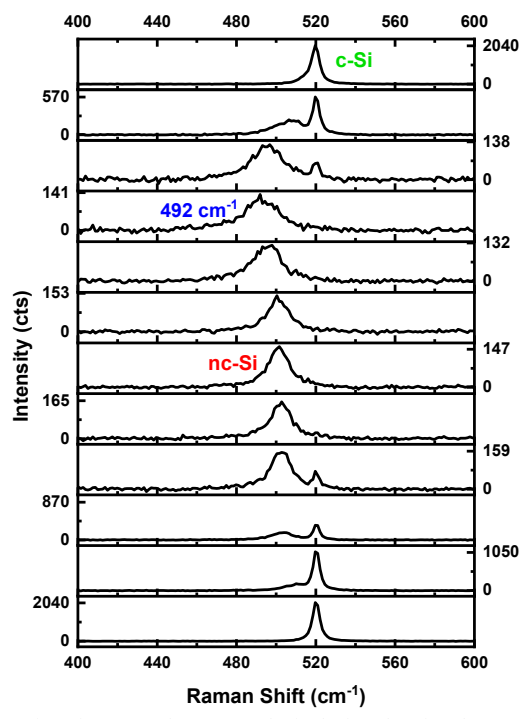


Fig. 3. A series of spectra taken across the inclusion showing the transition from c-Si to nc-Si and back to c-Si.

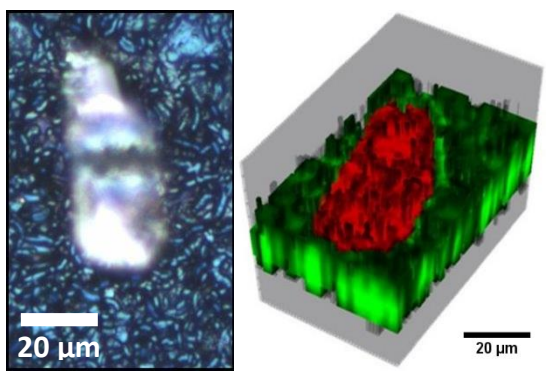


Fig. 4. 2D optical micrograph of the inclusion under the Raman microscope (left) and 3D Raman construction of the inclusion using confocal imaging (right).

Thus, confocal Raman microspectroscopy can be a powerful, non-destructive metrology tool to evaluate features in 3D as well as probe sub-surface features in Si solar cells.

Fig. 5A shows a Raman spectrum at the edge of the Ag finger shown in the inset with a '+' mark. The spectrum consists of two peaks. The primary peak is the TO phonon belonging to Si at 520.3 cm⁻¹ and the weaker, broader peak is at 680 cm⁻¹. The peak at 680 cm⁻¹ is attributed to the vibration of Ag[O-O]²⁻ bond in Ag₂O [5]. The origin of Ag₂O can be attributed to oxidation of Ag during the firing process. At distances \geq 15 μ m from the edge of the Ag line, the Si peak intensity is relatively uniform. As the laser approaches the Ag line, the Si peak intensity starts to decrease. Once the laser is atop the Ag line, the Si peak disappears completely, and the peak associated with Ag₂O (at 680 cm⁻¹) is visible only.

To establish the presence and extent of Ag₂O around the Ag line, we plot the Ag₂O peak intensity as an area map in Fig. 5B. The area mapping is obtained from the red boxed region in the inset of Fig. 5A. The dotted lines indicate the edges of the Ag finger and, where the Si peak intensity reaches zero. Clearly, the Ag₂O is detected well beyond the edges of the Ag line.

One possible reason for the presence of the Ag₂O away from the lines could be the initial application of Ag paste during the screen-printing process has a lateral spread greater than the

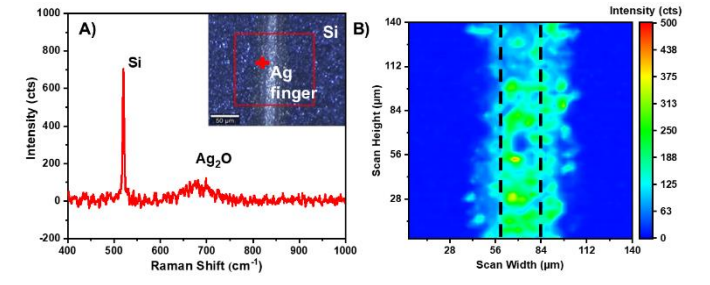


Fig. 5A. Raman spectrum of the silver line on the '+' mark in the inset shows two peaks – one at 520.3 cm⁻¹ corresponding to Si and another, weaker peak at 680 cm⁻¹ which corresponds to Ag₂O. 5B. The intensity map of the 680 cm⁻¹ peak is shown which appears concentrated above and in the vicinity of the silver line.

targeted line width ($\sim 30~\mu m$) obtained after the firing step. During the firing process, the volatile components are removed from the paste while the metallic components sinter and shrink laterally leaving residual Ag_2O behind. Thus, the mapping of Ag_2O beyond the Ag line can indirectly assess the quality and effectiveness of the firing process.

IV. SUMMARY

With the aim to highlight the utility of Raman as a characterization tool for Si solar cells, we have conducted Raman microspectroscopy on a multi crystalline Al-BSF solar cell. Three prototypical regions were scanned and analyzed. First, regions with remnant saw marks were observed where the peak were at higher wavenumbers and with wider FWHM compared to regions on textured multi crystalline Si surfaces with no saw marks. Next, an inclusion was characterized on the multi crystalline Si surface with the primary phase identified as nanocrystalline Si. The Si substrate around the inclusion was under tensile stress. Confocal mapping provided a nondestructive, 3D reconstruction of the inclusion, indicating the inclusion was embedded inside and protruded above the multi crystalline Si surface. Raman on Ag fingers indicated that Ag₂O could be detected up to 25 µm away from the line edges – a result of the screen-printing followed by firing process. Taken together, these results demonstrate the utility of Raman microspectroscopy in obtaining insights into the surface and sub-surface quality of Si solar cells, defect detection and process characterization.

ACKNOWLEDGMENT

This work was supported by the National Science Foundation (NSF) under Award Number 1562102. Use of HORIBA LabRam® confocal Raman is possible with support from NSF MRI Award Number 1920050.

REFERENCES

- [1] D. Quansah, M. Adaramola, G. Takyi and I. Edwin, "Reliability and Degradation of Solar PV Modules – Case Study of 19-Year-Old Polycrystalline Modules," Technologies, vol. 5, no. 2, 2017.
- [2] S. Banerjee, J. Yang, J.Wu, M. Heredia, Z. Gao, Y. Myung, O. Rezvanian and P. Banerjee, "Phase and stress evolution of Si swarf in the diamondcoated wire sawing of Si ingots," Int. J. Adv. Manuf. Technol., vol. 89, no. 1-4, pp. 735-742, 2016.
- [3] Z. Sui, P. P. Leong, I. P. Herman, G. S. Higashi, H. Temkin, "Raman analysis of light emitting porous silicon," Applied Physics Letters, vol. 60, no. 17, pp. 2086-2088, 1992.
- [4] J. Yang, S. Banerjee, J. Wu, Y. Myung, O. Rezvanian and P. Banerjee, "Phase and stress evolution in diamond microparticles during diamond-coated wire sawing of Si ingots," Int. J. Adv. Manuf. Technol., vol. 82, no. 9-12, pp. 1675-1682, 2015.
- [5] C.-B. Wang, G. Deo and I. E. Wachs, "Interaction of Polycrystalline Silver with Oxygen, Water, Carbon Dioxide, Ethylene, and Methanol: In Situ Raman and Catalytic Studies," J. Phys. Chem. B, vol. 103, no. 27, pp. 5645-5656, 1999.